Hybrid perovskites for photovoltaics: Insights from first principles

A. Filippetti and A. Mattoni

CNR-IOM, UOS Cagliari, c/o Dipartimento di Fisica, Università di Cagliari, S.P. Monserrato-Sestu Km. 0.700, Monserrato, Cagliari 09042, Italy

(Received 2 September 2013; revised manuscript received 15 January 2014; published 28 March 2014)

The methylammonium lead iodide perovskites at the core of recently proposed solar cells with exceptionally large quantum conversion efficiency are studied by first-principles methods. Large absorption coefficients (0.03–0.04 nm^{-1} for wavelength ∼500 nm) and small effective masses suited for both n-type and p-type transport are obtained as a consequence of their peculiar structural and electronic characteristics. In particular, the presence of a direct gap between highly dispersed Pb($6s$)-I($5p$) valence bands and Pb($6p$) conduction bands is the key ingredient at the basis of their excellent performance in photovoltaic applications.

DOI: 10.1103/PhysRevB.89.125203 PACS number(s): 73.50.Pz, 78.20.−e, 78.40.−q, 78.56.−a

I. INTRODUCTION

The last "mutation" (to quote Ref. [1]) in the breakneck run towards efficient and economically feasible photovoltaic devices spotlights the class of $M\mathrm{PbI}_{3-x}\mathrm{Cl}_x$ hybrid (i.e., mixed organic-inorganic) perovskites, where M labels the methylammonium molecule (CH_3-NH_3) located at the A site of the perovskite. These systems can be processed quite inexpensively from solution (e.g., by printing) at low temperature, creating novel opportunities for competitive mass-production solar cell technology.

In several recent works, highly efficient sunlight-converting devices based on $M\mathrm{PbI}_3$ [2–10], $M\mathrm{PbBr}_3$ [7,8,10,11], and $M\mathrm{PbI}_{3-x}\mathrm{Cl}_x$ [12,13] as the light absorber were presented. Impressively, in some of these experiments the perovskite acts as both optically active and charge transport material. This multifunctional capability overcomes the problem of energy losses at the absorber/conductor interface. For example, power-conversion efficiency (PCE) of 8% was obtained [12] in a single-junction device using $M\mathrm{PbI}_2\mathrm{Cl}$ as the light absorber, with mesoporous TiO_2 and spiro-OMeTAD polymer as the n-type and p-type conductors, respectively. However, upon substitution of TiO_2 with the wide-gap Al_2O_3 purely acting as a scaffold and forcing the current to remain confined in the perovskite, PCE rose up to a remarkable 10.9%, suggesting that the perovskite is not only an efficient optical absorber but even a good n-type conductor. Later works [13–15] proposed new processing methods and device architectures capable of further pushing the device efficiency up to above 15%, and showed that perovskite thin films enable photogeneration and transport of both n-type and p-type carriers with internal quantum efficiency close to 100%. In other experiments [4], solar cells based on the $M\mathrm{PbI}_3/TiO_2$ heterojunction with the perovskite used as both light absorber and hole conductor reached PCE between 5.5% and 7.3%, and very recently a record-high 15% PCE was reported for a $M\mathrm{PbI}_3/TiO_2$ solar cell [9], as a result of novel sequential deposition techniques improving the morphological homogeneity of the perovskite. To further attest to the universal quality of these perovskites, a noticeable 12% efficiency was recently obtained using organic charge-transport layers [16] in place of the usual oxides, and about 14% upon substitution of methylammonium with formamidinium [17].

All these results coherently point to $M\mathrm{PbI}_{3-x}\mathrm{Cl}_x$ as the first materials to emerge which possess all the required features for efficient solar cell applications: low-cost processing, capability of light absorption and carrier generation, and good transport properties for both hole and electron carriers. It is thus timely for this theory to shed light on the reasons for these performances from a fundamental viewpoint. Recent theoretical works report detailed *ab initio* calculations for hybrid perovskites, focusing on their structural [18–21], electronic [18,20,22–25], and vibrational [26] properties. However, a clear understanding of what is really special about these materials is, in our opinion, still missing.

In this work we focus in particular on the description of the optical absorption of $M\mathrm{PbI}_3$ and $M\mathrm{PbI}_2\mathrm{Cl}$. In general, our aim is to unveil, from a fundamental viewpoint, the mechanisms which relate the basic properties of these systems with the observed optical and transport behavior. We will provide evidence that the excellent performances of these systems are primarily related to the absolute predominance of the Pb^{2+} $6s$ state at the valence band top and the Pb $6p$ states at the conduction band bottom. These fairly extended orbitals give rise to broadly dispersed bands with light masses at the band extrema, which indicate the possibility of good electron and hole mobility. Moreover, our calculations attest to an absorbance comparable to that of the best semiconducting absorbers. The role of the molecule in these performances is also well described by our results. On the one hand, the molecule donates an electron to the halogen ions while its electronic levels do not directly couple with the bands derived from the inorganic side, remaining well separated in energy from the important region of the photoabsorption process. On the other hand, however, the orientation of the molecules does play an important role with regard to the atomic structure (and the octahedral rotations in particular), thus indirectly affecting the electronic properties as well.

II. METHOD

For our calculations we used the local density functional theory (LDA), implemented in a plane-wave basis set and ultrasoft pseudopotentials [27]. We verified that this approach accurately describes the atomic structure of the isolated molecule. We also used the variational pseudo-self-interaction correction (VPSIC) [28] as a check of the electronic states of the molecule. Optical properties are obtained in random-phase

approximation from the band energies calculated on a very dense k-point mesh.

III. RESULTS

A. Structure

We assume the tetragonal $I4/mcm$ symmetry proper of these systems at room temperature ($\sqrt{2} \times \sqrt{2} \times 2$ 48-atom unit cells) and cell parameters taken from experiments (for MPbI$_3$ [29–31] $a_0 = 8.80$ Å, $c_0 = 12.68$ Å; for MPbI$_2$Cl [12] $a_0 = 8.83$ Å, $c_0 = 11.24$ Å), whereas the atomic structure is fully optimized by total energy minimization. For the molecule we tested various possible high-symmetry high-entropy configurations as a starting point, with M centered on the A site and the C-N axis parallel to the [110], [111], and [100] directions. After full atomic relaxation, the structures shown in Fig. 1 resulted as the most stable. In MPbI$_3$, M is nearly aligned along the [110] direction, parallel to the Pb-I-Pb bonds; in MPbI$_2$Cl the molecule is also slightly tilted out of plane due to the stronger tetragonal anisotropy. Our atomic structure for MPbI$_3$ is in good agreement with the measurements of Ref. [29].

Concerning the difference between the two compounds, it is apparent from the top view that MPbI$_2$Cl presents smaller octahedral rotations in the (001) plane, i.e., larger planar Pb-I-Pb angles (153°) than MPbI$_3$ (147°). This can be understood in terms of the different ionic radius for I^{1-} (2.06) and Cl^{1-} (1.67), which reverberates in different tolerance factors [32] (see Appendix B for a detailed description) and c_0/a_0 ratio (1.02 and 0.9, respectively). Thus while the former is close to cubic, MPbI$_2$C is highly anisotropic and remarkably squeezed along [001], whereas a_0 is similar for the two compounds.

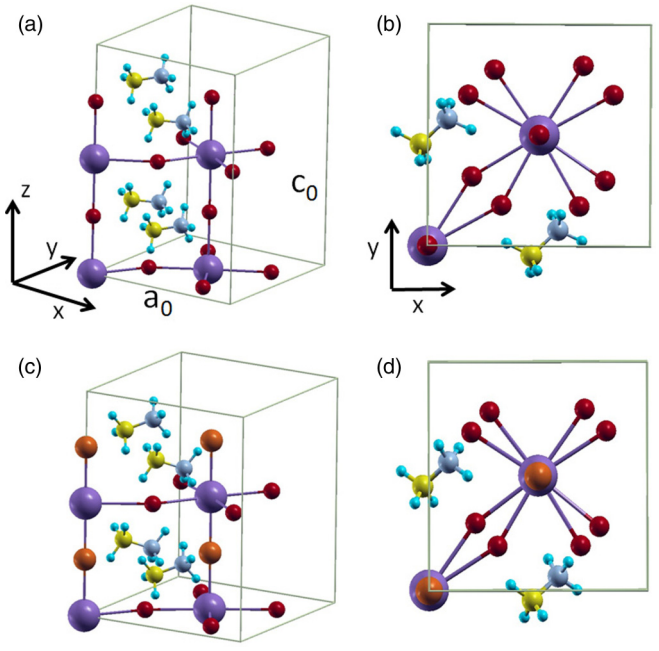

FIG. 1. (Color online) Top panels: Three-dimensional view (left) and top-view (right) of the unit cell for MPbI$_3$. Bottom panels: same for MPbI$_2$Cl. Color code: yellow (C), gray (N), cyan (H), red (I), violet (Pb), orange (Cl).

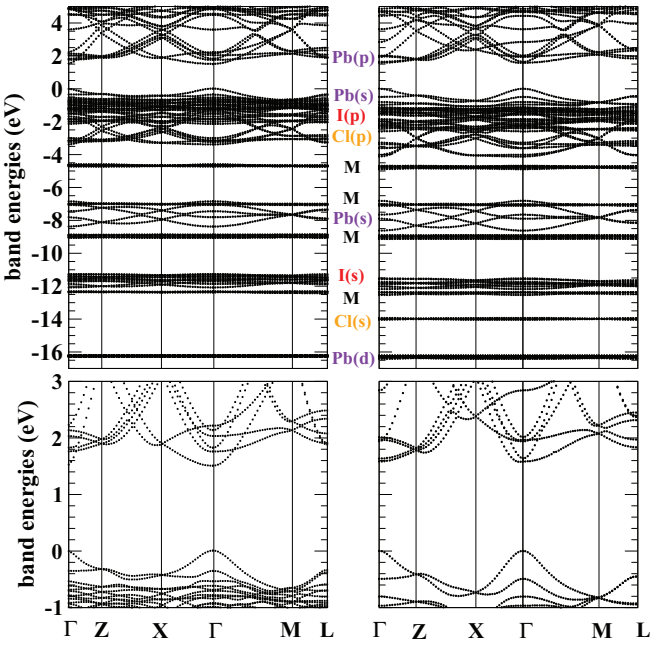

FIG. 2. (Color online) Calculated band energies for MPbI$_3$ (left) and MPbI$_2$Cl (right panels). Labels indicate the atomic and orbital character for each group of bands (M labels molecular states). In the bottom panels the enlargement around the band gap is shown. k-point coordinates (unit of $2\pi/a$) are $X = (1/2,0,0)$, $L = (1/2,1/2,0)$, $M = (1/2,1/2,a/2c)$, $Z = (0,0,a/2c)$.

B. Electronic properties

In Fig. 2 we report the band structure calculated for MPbI$_3$ and MPbI$_2$Cl, respectively. Both systems are semiconductors with a fundamental band gap equal to 1.51 eV for MPbI$_3$ and 1.57 eV for MPbI$_2$Cl [zero energy is fixed at the valence band top (VBT)], in excellent agreement with the value inferred from the measured absorption onset (1.55 eV [12]). For both systems the gap is direct at the Γ point. In the figure, the atomic character for each group of bands is also indicated. The quantum chemistry of these systems is well captured by the calculated orbital-projected density of states (DOS) in Fig. 3. The integrals of the DOS components show that the ionic charges are close to the expected nominal ionic picture: M^{1+}, Pb^{2+}, I^{1-}, and Cl^{1-}.

From band energies and DOS spectra, the occupied molecular states are easily recognizable as four perfectly flat horizontal lines in the band structure, and four corresponding vertical lines in the DOS; this indicates that the electronic states of the molecule remain well localized in space, without substantial hopping with the surrounding inorganic environment. Moreover, these states are far below the energy gap region which controls the photoconversion properties: the energy-highest occupied (HOMO) M^{1+} level lies ∼5 eV below the VBT. Concerning the empty M states, they only appear above 3.5 eV, that is 2 eV above the conduction band bottom (CBB). From this result we can infer a first paramount characteristic of these hybrid systems: Organic and inorganic sides are basically decoupled from the electronic viewpoint, and thus the molecule does not interfere with the active region of the perovskite. Its only role, with regard

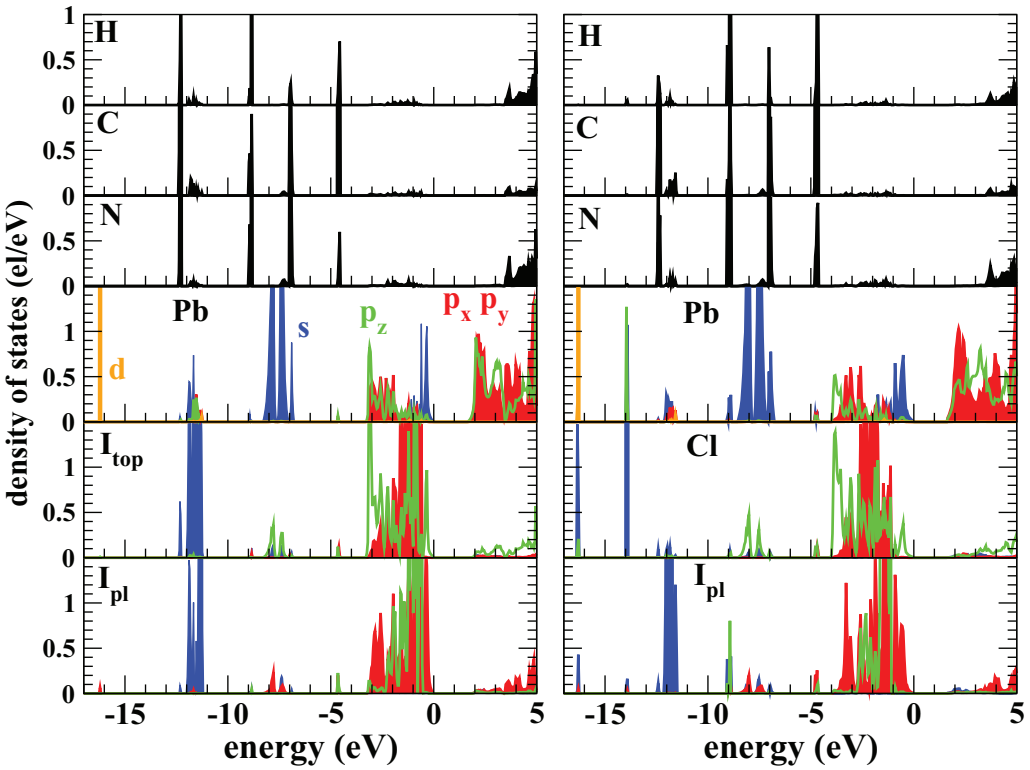

FIG. 3. (Color online) Atomic- and orbital-projected DOS for MPbI$_3$ (left panels) and MPbI$_2$Cl (right panels). Each panel refers to the atomic species indicated by the label. Orbital contributions are represented by different colors: s states in blue, p_x-p_y states in red, p_z states in green, and d states in orange. For the molecule, sp^3 states are in black.

to the electronic properties, is to donate one electron to the surrounding environment.

Consider that the HOMO of neutral M is located ∼10 eV above the M^{1+} HOMO, thus ∼4 eV above the I and Cl p-type valence band top (see the DOS in Fig. 3). This large difference between the M and M^{1+} HOMO levels ultimately motivates the electron transfer from the molecule to the inorganic side and in turn the insulating character of the perovskite. This brings us to the second key element of our results: Pb^{2+} states govern the energy-conversion properties of these systems. The VBT is characterized by hybridized Pb($6s$)-I/Cl($5p$) states, while the CBB is of pure Pb($6p$) character; thus the low-energy absorption region is Pb dominated. The large bandwidth of these states is coherent with the good transport properties argued for both types of carriers.

It is important to emphasize the general validity of this picture: (i) it equally holds for MPbI$_3$ and MPbI$_2$Cl; (ii) it does not depend on the specific M orientation or on the details of the atomic structure (other structural local minima with different M orientations held a similar DOS); and (iii) it is not an artifact of LDA (calculations done by the VPSIC approach obtain similar results). Notice, however, that the role of M is not irrelevant in the photoconversion efficiency, since it directly influences the structural properties which in turn determine the electronic properties as well. As an example, we verified that a different M orientation with the dimers parallel to the [100] direction may reduce the octahedral rotations, and in turn increase the Pb(s)-I(p) hopping and bandwidth. Despite those large structural effects, the M^{1+} HOMO energy remains equally far below the band-gap region. (The case of a [100]-oriented molecule is described in detail in Appendix A.)

Concerning the calculated band masses, starting from the conduction bands, we find that MPbI$_3$ displays a very light electron mass along z ($m_{zz} = 0.14$ in electron mass units) and heavier masses in plane ($m_{xx} = m_{yy} = 2.19$). Since this system is chemically isotropic, the mass anisotropy spurs entirely from the different octahedral rotations. Pb-I-Pb segments are straight along z, thus favoring large Pb(p_z)-Pb(p_z) hopping and in turn large bandwidth, while in the (001) plane they form angles of 147°; thus a large deviation from the ideal 180° value leads to reduction of hopping and bandwidth. In MPbI$_2$Cl, on the other hand, the c/a shrinking and the smaller octahedral rotations stabilize the planar Pb p_x and p_y states over the p_z state. Thus the formers dominate the energy region between 1.5 and 3 eV (see the DOS in Fig. 3). Now the mass is heavy along z ($m_{zz} = 2.71$), while in the plane two light masses (0.21 and 0.59) are found, relative to two Pb p_x-p_y bands separated by 0.1 eV. Concerning the valence bands (i.e., p-type transport), both compounds show large bandwidth, in turn due to the large Pb(s)-I(p) orbital hybridization which characterizes the VBT. Due to the smaller octahedral rotations, MPbI$_2$Cl is the system with the lightest masses ($m_{xx} = m_{yy} = 0.51$, $m_{zz} = 0.67$).

We can summarize our band energy results as follows: Structural differences between MPbI$_3$ and MPbI$_2$Cl induce sizable differences in electronic and transport properties as well. For n-type transport, MPbI$_3$ and MPbI$_2$Cl are expected to have good mobility in one and two dimensions, respectively. This result indicates that MPbI$_2$Cl may be best suited as an n-type conductor in layered heterostructures. On the other hand,

both perovskites are expected to be good hole conductors, although MPbI$_2$Cl may arguably display higher hole mobility due to slightly lower effective masses.

C. Optical properties

Here we illustrate the calculated optical properties for MPbI$_3$ and MPbI$_2$Cl, reported in Fig. 4. For both systems

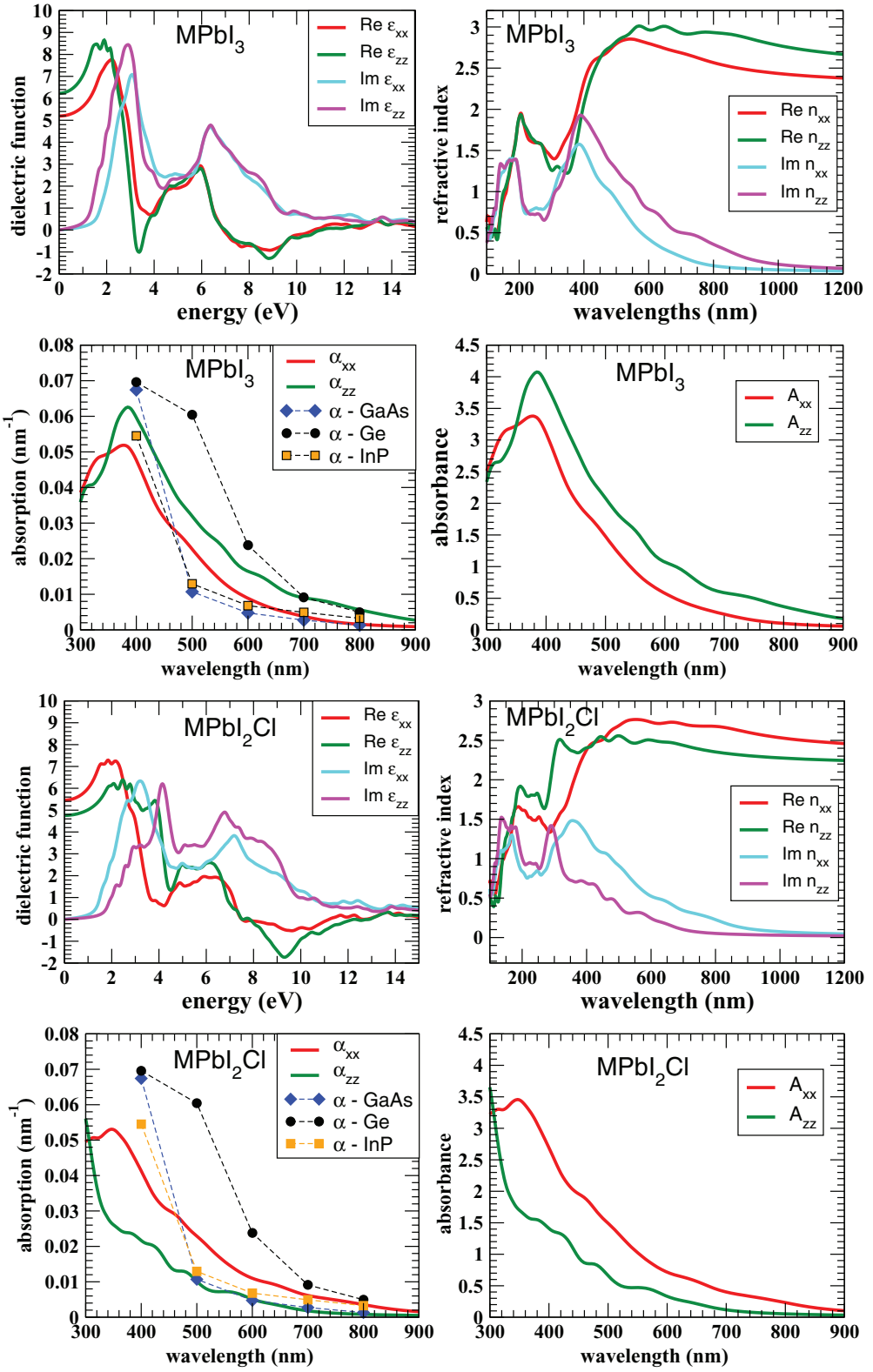

FIG. 4. (Color online) Calculated optical properties for MPbI$_3$ and MPbI$_2$Cl: real and imaginary dielectric function (ϵ), refractive index (n), absorption coefficient (α), and absorbance (A) through a perovskite film of 150 nm (see text). For each quantity, planar ($xx = yy$) and orthogonal (zz) components are separately shown. Absorption for typical semiconductors [33] is reported for comparison.

we can observe a large tetragonal anisotropy in both dielectric function (ϵ) and refractive index (n). The two systems show largely different anisotropy since for MPbI$_3$, z is the direction with larger reflectivity and absorption, while for MPbI$_2$Cl the planar components prevail, consistent with what we have seen for the electronic properties. Regarding absorption (α), which is our primary interest here, the most striking result is the large calculated value (up to 0.05–0.06 nm^{-1}) in the 400–800 nm wavelength range for both perovskites. We also report absorption values for some typical semiconductors (GaAs, Ge, InP) [33]. We see that both perovskites compare very well with these prototypical optical absorbers, not only in the infrared region (above 700 nm), but even in the visible range from 500 nm and beyond, i.e., in the spectrum region of maximum sunlight irradiance. This striking result is favored by the perovskite band structure. The band gap is direct and occurs at the Γ point; thus a very robust absorption process starts immediately at the onset of the fundamental interband transition (1.51 eV, corresponding to 820 nm for MPbI$_2$Cl).

To quantify the performance of the perovskites in actual devices and have a meaningful term of comparison with the experiments, we also report the absorbance A [34] calculated over a perovskite film thickness of $L = 150$ nm reported in Ref. [12]. The curves calculated for A_{zz} for MPbI$_3$ and $A_{xx} = A_{yy}$ for MPbI$_2$Cl are both in reasonable agreement with the measurement of Ref. [12]. For example, they measure $A = 1.8$ at 500 nm, against our calculated values of $A = 2.2$ and 1.4 for MPbI$_3$ and MPbI$_2$Cl, respectively. This is a quite satisfying agreement, considering that our calculations deal with intrinsic bulk systems, while actual samples may be affected by structural and chemical inhomogeneity or disorder. Notice that $A = 2.2$ and 1.4 correspond to very large relative absorptions $I/I_0 = 10^{-A}$ (99.3% and 96%, respectively).

IV. CONCLUSIONS

In summary, we studied MPbI$_3$ and MPbI$_2$Cl perovskites from first-principles calculations. Our description of band-gap and optical absorbance agrees nicely with available experiments. Moreover, our analysis relates the exceptional behavior of these materials with their basic structural and electronic characteristics, thus drawing useful guidelines for the search of alternative materials with improved performances.

Several major conceptual conclusions were reached: (i) Optical and transport properties are substantially independent of the electronic states of the molecule. This decoupling is a direct consequence of the fact that the electronic energies of the molecule are well separated from the important region (i.e., the band gap) which governs optical and transport properties. In other words, M acts as a pure donor whose electronic levels do not directly couple with the bands involved in optical and transport properties. (ii) Nevertheless, albeit indirectly, the orientation of M can significantly reverberate on optics and transport, since it largely affects the amplitude of the octahedral rotations, which in turn governs Pb-I-Pb hopping and ultimately the Pb bandwidth. (iii) Pb^{2+} ion plays a paramount role in the optical properties of these systems since the band gap (direct at Γ point) opens between Pb($6s$)-I($5p$) valence states and a conduction band manifold of exclusively Pb($6p$) character. Thus the delocalized character of these orbitals is the basis of the large optical absorption in both the visible and infrared range. Not by chance, this fortunate presence of delocalized Pb s states at the VBT is shared by other plumbates (PbS, PbSe, PbTe), popularly regarded as promising vehicles of photoconversion efficiency [35–38].

Finally, it is useful to emphasize the key difference of these perovskites with the much more popular oxide perovskites (e.g., titanates, manganites, or nickelates): in the latter, the band gap opens between fairly localized O($2p$) valence and B-site ($3d$) conduction bands. As a consequence, the charge mobility at the band edges is not particularly satisfying, and the typically small bandwidth does not play favorably for absorption in the useful spectral region.

ACKNOWLEDGMENTS

This work was supported in part by the MIUR-PRIN 2010 *Oxide*, IIT-Seed NEWDFESCM, IIT-SEED POLYPHEMO, and "platform computation" of IIT, Fondazione Banco di Sardegna, Regione Autonoma della Sardegna, under L.R. 7/2007 (CRP-18013, CRP-24978), ISCRA computing projects "SpinOx" and "SuperFET" at CINECA, CRS4 and Cybersar computing resources in Cagliari.

APPENDIX A: ELECTRONIC PROPERTIES OF MPbI$_2$Cl WITH [100]-ORIENTED MOLECULES

In the following we describe the electronic properties calculated for MPbI$_2$Cl, still within the tetragonal $I4/mcm$ structure stable at room temperature but with the molecules oriented along the [100] direction. After atomic position optimization, we found the energy of this structure to be higher than that of the [110] ground state by only 3.2 meV/f.u. Thus, they are almost degenerate, and both can be significant at low temperature. In fact, the thermodynamic average of electronic properties over different static molecular orientations may furnish the closest representation to the actual system. Among high-symmetry molecule configurations we also considered [111]-oriented molecules; however, after structural optimization we found this configuration to be much higher in energy (43.9 meV/f.u. higher than the [110] ground state), and thus it is not considered here.

In Fig. 5 the orbital- and atom-resolved DOSs for MPbI$_2$Cl with [100]-oriented molecules are shown. We see that all the important characteristics described in the main article for the [110] orientation can be replicated for this structure as well. In particular, the occupied molecular states (drawn in black) are all quite flat and located far below the valence band top (VBT), with the exception of a small DOS pocket derived from C and N atoms within the [–3 eV, –1 eV] range. It follows that (a) the overlap between molecular orbitals and extended states is discardable or marginal, and (b) the electronic states of the molecule do not directly affect the optical and transport properties of the perovskite.

A sensible difference between [100] and [110] configurations resides in the band gap. For the former structure, this is remarkably smaller (1.25 eV, vs 1.57 eV calculated for the latter) as a consequence of the smaller octahedral rotation (explained in the next section), and thus there is a larger bandwidth and in-plane Pb-I orbital hybridization. Clearly, a smaller band gap reverberates in a larger wavelength onset

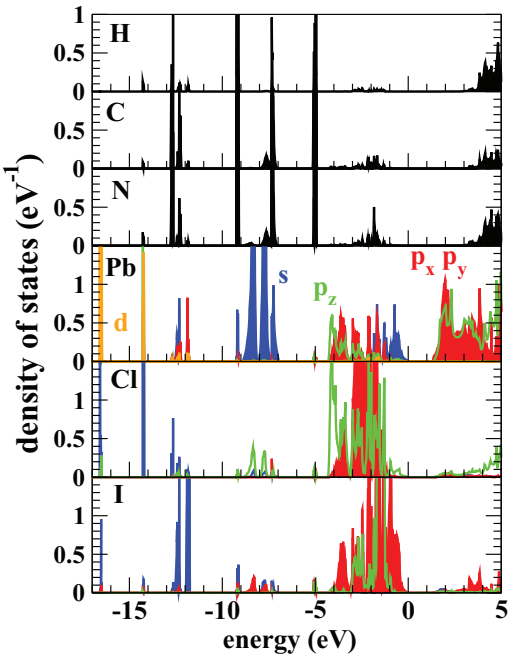

FIG. 5. (Color online) Atomic- and orbital-projected DOS for $M\mathrm{PbI_2Cl}$ with the molecule oriented along the [100] direction. Each panel refers to the atomic species indicated by the black label. The orbital character is indicated by labels of corresponding color: s states in blue, p_x-p_y states in red, p_z states in green, and d states in orange. For the molecule, sp^3 states are in black.

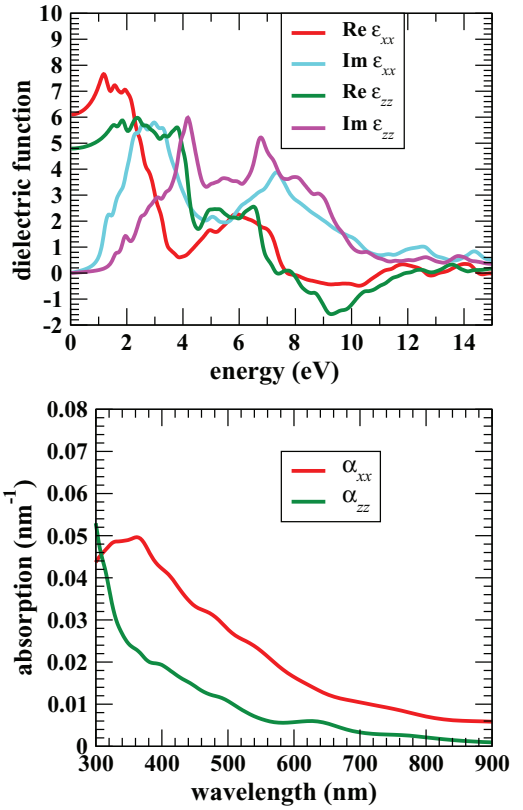

FIG. 6. (Color online) Calculated optical properties for the [100]-oriented $M\mathrm{PbI_2Cl}$. Top panel: real and imaginary dielectric function (ϵ). Bottom: absorption coefficient (α). For each quantity, planar ($xx = yy$) and orthogonal (zz) components are separately shown.

for photoabsorption; however, the shape and amplitude of absorption (see Fig. 6) in the relevant range of frequency remain very similar to those obtained for the [110] molecular orientation. There is a strong tetragonal anisotropy in both dielectric function (ϵ) and optical absorption (α). For the latter, the planar components are visibly larger than the orthogonal component, reaching values as large as $\sim$0.04–0.05 nm^{-1} at about 400 nm wavelength.

These results strengthen the concept that the excellent optical properties of the hybrid perovskites are rather unaffected by the specific orientation of the molecule. We emphasize that this aspect is instrumental to effective performance in actual devices, where the molecular orientation is arguably quenched by thermal fluctuations, as well as configurational and structural disorder.

APPENDIX B: STRUCTURES AND TOLERANCE FACTORS

In this work we have considered three systems, namely, $M\mathrm{PbI_3}$ and $M\mathrm{PbI_2Cl}$ with [110]-oriented molecules, and $M\mathrm{PbI_2Cl}$ with [100]-oriented molecules, all within tetragonal $I4/mcm$ symmetry found by the experiment as the stable structure at room temperature. $I4/mcm$ symmetry is characterized by octahedral rotations labeled $a^0a^0c^-$ (in Glazer notation), which indicates no rotation along the $a = b$ axes, and antiphase rotations along c. (Here a, b, c refer to the conventional cubic cell, which is 45° rotated in the (a,b) plane with respect to the tetragonal unit cells.) Thus once the cell parameters are fixed, only one more internal degree of freedom, namely, the octahedral rotation in the (a,b) plane, is left to be further optimized.

In Fig. 7 we report the relaxed structures for these three perovskites, with both a cubic and rotated reference system indicated. These structures are obtained as follows: At the beginning of the relaxation procedure the molecule is placed with the C-N axis parallel to the [100] or [110] direction, and the other atoms in cubic octahedral positions; then we leave all the atoms to freely relax to the energy minimum. We see that at the end of relaxation, the [100]-oriented molecules are actually slightly titled in the (001) plane with respect to the [100] direction, and the [110]-oriented molecules also tilted out the (001) plane. However, for the sake of simplicity, we label them according to their starting orientations, [100] and [110]. We see in the figure that the three structures are characterized by quite different Pb-I-Pb angles: close to flat (170°) for the $M\mathrm{PbI_2Cl}$ [100], and remarkably rotated for the two [110] systems (153° and 147° for $M\mathrm{PbI_2Cl}$ and $M\mathrm{PbI_3}$, respectively).

In order to reach a qualitative understanding of the perovskite structure, a typically useful parameter is the tolerance factor, introduced by Goldsmith in 1926 [32], which quantifies the structural misfit by treating the ions as packed rigid spheres. For the ABX_3 perovskite it is

$$t = \frac{r_A + r_X}{\sqrt{2}(r_B + r_X)}, \tag{B1}$$

where r_A, r_B, and r_X are ionic radii of ions A, B, and X. Typically, a tolerance factor lower than $\sim$0.9 indicates the tendency

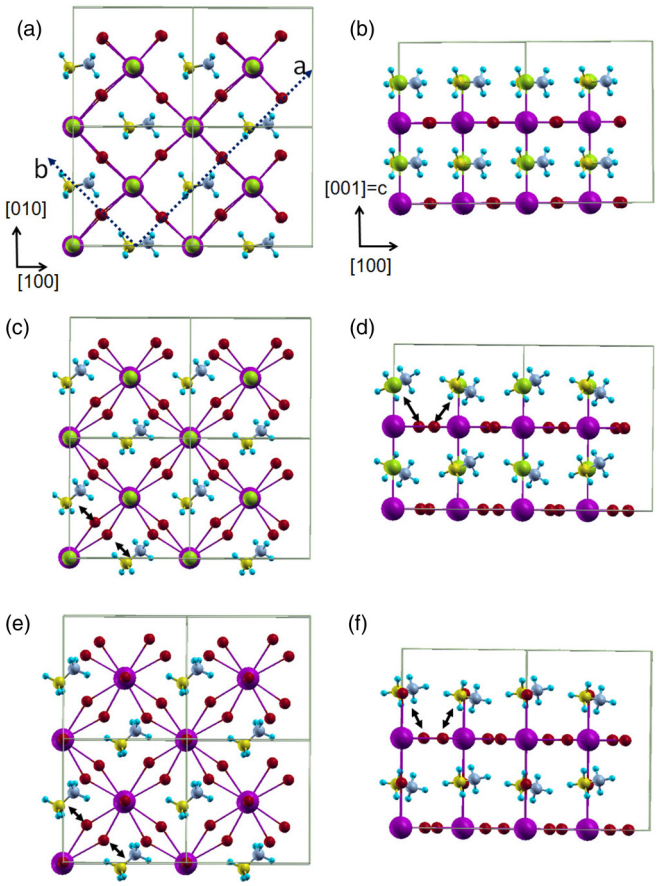

FIG. 7. (Color online) Structure of the $2\sqrt{2} \times 2\sqrt{2} \times 2$ supercell for [100]-oriented $M\mathrm{PbI_2Cl}$ [panels (a) and (b)], [110]-oriented $M\mathrm{PbI_2Cl}$ [panels (c) and (d)], and [110]-oriented $M\mathrm{PbI_3}$ [panels (e) and (f)]. The reference system indicated by black solid arrows refers to the $\sqrt{2} \times \sqrt{2} \times 2$ tetragonal unit cell, while a and b are 45°-rotated axes of the conventional cubic cell. Small arrows indicate the important M-I distances shortened by the octahedral rotations (see text). Atomic colors are yellow (C), gray (N), cyan (H), red (I), violet (Pb), green (Cl).

of loosing the ideal cubic symmetry, and movement towards low-symmetry tetragonal, orthorhombic, or rhombohedral structures characterized by cooperative octahedra rotations. In the present case, however, two additional ingredients complicate the picture: (a) the chemical mixture of Cl and I ions and (b) the nonsphericity of the molecule. Clearly, factor (a) is a determinant to distinguishing the tolerance factors of [110] $M\mathrm{PbI_3}$ and $M\mathrm{PbI_2Cl}$ systems, while (b) distinguishes the cases of [100] and [110] $M\mathrm{PbI_2Cl}$.

To include these ingredients in the tolerance factor, we considered the following generalization: For each structure, three inequivalent planes [(a,b), (a,c), and (b,c)] and three corresponding tolerance factors (t_{ab}, t_{ac}, t_{bc}, respectively) are defined as (now $A = M$ and $B = \mathrm{Pb}$, $X = \mathrm{I}$ or Cl)

$$t_{ab} = \frac{r_M^{ab} + r_{\mathrm{Cl}}}{r_{\mathrm{Pb}} + r_{\mathrm{I}}} \cos(\theta_{ab}), \quad t_{ac} = \frac{r_M^{ac} + r_{\mathrm{I}}}{r_{\mathrm{Pb}} + r_{\mathrm{I}}} \cos(\theta_{ac}),$$
$$t_{bc} = \frac{r_M^{bc} + r_{\mathrm{I}}}{r_{\mathrm{Pb}} + r_{\mathrm{I}}} \cos(\theta_{bc}), \tag{B2}$$

where θ is the plane-diagonal angle expressed in terms of ionic radii: $r_{\mathrm{Pb}} = 1.33$ Å for Pb^{2+}, $r_{\mathrm{I}} = 2.06$ Å for I^{1-}, $r_{\mathrm{Cl}} = 1.67$ Å for Cl^{1-}. The geometrical factor $\cos(\theta)$ takes into account the fact that the plane may not be squared, due to the presence of two different anions (I and Cl) in the same face:

$$\theta_{ab} = \tan^{-1}\left(\frac{r_{\mathrm{Pb}} + r_{\mathrm{I}}}{r_{\mathrm{Pb}} + r_{\mathrm{I}}}\right) = 45^\circ,$$
$$\theta_{ac} = \tan^{-1}\left(\frac{r_{\mathrm{Pb}} + r_{\mathrm{Cl}}}{r_{\mathrm{Pb}} + r_{\mathrm{I}}}\right), \tag{B3}$$
$$\theta_{bc} = \theta_{ac}.$$

Thus for (a,b) or any plane of the $M\mathrm{PbI_3}$ perovskite, $\cos(\theta) = 1/\sqrt{2}$ and the tolerance factor goes back to the standard expression.

Furthermore, in Eqs. (B2) we introduced a plane-dependent effective ionic radius for the molecule in order to include the effect of different orientations:

$$r_M^{ab} = \frac{d}{2}\cos(\alpha) + r_{\mathrm{N}}, \quad r_M^{ac} = \frac{d}{2}\cos(\beta) + r_{\mathrm{N}},$$
$$r_M^{bc} = \frac{d}{2}\cos(\gamma) + r_{\mathrm{N}},$$

where $d = 2.47$ Å is the molecule length, $r_{\mathrm{N}} = 1.32$ Å for N^{3-}, and the cosines project the dimer direction onto the molecule-anion distance on each plane. Clearly, for spherically averaged molecules, the effective radii are all equal and the standard definition is recovered.

In Table I we report the calculated parameters for each considered structure. The key quantity to explain the different rotation amplitude of the examined perovskites is t_{bc}, very small for the two [110] structures and fairly large for the [100]. The reason can be easily understood by looking at Fig. 7. For the [100] orientation (panels A and B), planes (a,c) and (b,c) are nearly equivalent; on the contrary, for the [110] orientation, (a,c) and (b,c) are quite different due to the asymmetric orientation of the molecules along axes

TABLE I. Generalized tolerance factors t, angles, and effective molecular radius r_M^{ab} (Å) for the three perovskites considered in the article. The definitions are given in the text.

	$M\mathrm{PbI_2Cl}$ [100]	$M\mathrm{PbI_2Cl}$ [110]	$M\mathrm{PbI_3}$ [110]
t_{ab}	0.88	0.81	0.89
t_{ac}	0.94	1.02	0.96
t_{bc}	0.94	0.75	0.71
θ_{ab}	45°	45°	45°
θ_{ac}	41.5°	41.5°	45°
θ_{bc}	41.5°	41.5°	45°
α	0	45°	45°
β	45°	0	0
γ	45°	90°	90°
r_M^{ab}	2.55	2.19	2.19
r_M^{ac}	2.19	2.55	2.55
r_M^{bc}	2.19	1.32	1.32

a and b. The visible emptiness present in the (b,c) planes between ions M and I produces very small t_{bc}. This emptiness is compensated by octahedral rotations parallel to (a,b), which reduce the M-I distances (see the small black arrows in the figure). Conveniently, the model also distinguishes between [110] $M\mathrm{PbI_2Cl}$ and $M\mathrm{PbI_3}$ systems: while they have the same molecule effective radius, t_{bc} is slightly smaller for the latter, due to the fact that $r_\mathrm{I} > r_\mathrm{Cl}$.

Finally, it is interesting to notice that even t_{ab} is rather small, albeit larger than t_{bc}, in all the considered systems. This signals the tendency of developing octahedral rotations which could close the space between M and Cl (or I for $M\mathrm{PbI_3}$) in the (a,b) planes. These rotations around the a and b axes are ruled out in tetragonal symmetry but can be activated by a structural transition to orthorhombic symmetry, which is known to occur for these hybrid perovskites at lower temperature.

[1] D. J. Norris and E. S. Aydil, Science **338**, 625 (2012).

[2] J.-H. Im, C.-R. Lee, J.-W. Lee, S.-W. Park, and N.-G. Park, Nanoscale **3**, 4088 (2011).

[3] H.-S. Kim, C.-R. Lee, J.-H. Im, K.-B. Lee, T. Moehl, A. Marchioro, S.-J. Moon, R. Humphry-Baker, J.-H. Yum, J. E. Moser, M. Grätzel, and N.-G. Park, Sci. Rep. **2**, 591 (2012).

[4] L. Etgar, P. Gao, Z. Xue, Q. Peng, A. K. Chandiran, B. Liu, Md. K. Nazeeruddin, and M. Grätzel, J. Am. Chem. Soc. **134**, 17396 (2012).

[5] H. Chen, X. Pan, W. Liu, M. Cai, D. Kou, Z. Huo, X. Fang, and S. Dai, Chem. Commun. **49**, 7277 (2013).

[6] D. Bi, L. Yang, G. Boschloo, A. Hagfeldt, and E. M. J. Johansson, J. Phys. Chem. Lett. **4**, 1532 (2013).

[7] B. Cai, Y. Xing, Z. Yang, W.-H. Zhang, and J. Qiu, Energy Environ. Sci. **6**, 1480 (2013).

[8] J. Qiu, Y. Qiu, K. Yan, M. Zhong, C. Mu, H. Yan, and S. Yang, Nanoscale **5**, 3245 (2013).

[9] J. Burschka, N. Pellet, S.-J. Moon, R. Humphry-Baker, P. Gao, M. K. Nazeeruddin, and M. Grätzel, Nature (London) **499**, 316 (2013).

[10] A. Kojima, K. Teshima, Y. Shirai, and T. Miyasaka, J. Am. Chem. Soc. **131**, 6050 (2009).

[11] E. Edri, S. Kirmayer, D. Cahen, and G. Hodes, J. Phys. Chem. Lett. **4**, 897 (2013).

[12] M. M. Lee, J. Teuscher, T. Miyasaka, T. N. Murakami, and H. J. Snaith, Science **338**, 643 (2012).

[13] J. M. Ball, M. M. Lee, A. Hey, and H. J. Snaith, Energy Environ. Sci. **6**, 1739 (2013).

[14] M. Liu, M. B. Johnston, and H. J. Snaith, Nature (London) **501**, 395 (2013).

[15] D. Liu and T. L. Kelly, Nat. Photon. **8**, 133 (2014).

[16] O. Malinkiewicz, A. Yella, Y. H. Lee, G. M. Espallargas, M. Grætzel, M. K. Nazeeruddin, and H. J. Bolink, Nat. Photon. **8**, 128 (2014).

[17] G. E. Eperon, S. D. Stranks, C. Menelaou, M. B. Johnston, L. M. Herz, and H. J. Snaith, Energy Environ. Sci. **7**, 982 (2014).

[18] Y. H. Chang, C. H. Park, and K. Matsuishi, J. Korean Phys. Soc. **44**, 889 (2004).

[19] E. Mosconi, A. Amat, M. K. Nazeeruddin, M. Grätzel, and F. De Angelis, J. Phys. Chem. C **117**, 13902 (2013).

[20] F. Brivio, A. B. Walker, and A. Walsh, APL Mater. **1**, 042111 (2013).

[21] S. Colella, E. Mosconi, P. Fedeli, A. Listorti, F. Gazza, F. Orlandi, P. Ferro, T. Besagni, A. Rizzo, G. Calestani, G. Gigli, F. De Angelis, and R. Mosca, Chem. Mater. **25**, 4613 (2013).

[22] I. B. Koutselasy, L. Ducassez, and G. C. Papavassiliou, J. Phys.: Condens. Matter **8**, 1217 (1996).

[23] J. Even, L. Pedesseau, J.-M. Jancu, and C. Katan, J. Phys. Chem. Lett. **4**, 2999 (2013).

[24] Y. Wang, T. Gould, J. F. Dobson, H. Zhang, H. Yang, X. Yao, and H. Zhao, Phys. Chem. Chem. Phys. **16**, 1424 (2014).

[25] P. Umari, E. Mosconi, and F. De Angelis, arXiv:1309.4895 (2013).

[26] C. Quarti, G. Grancini, E. Mosconi, P. Bruno, J. M. Ball, M. M. Lee, H. J. Snaith, A. Petrozza, and F. De Angelis, J. Phys. Chem. Lett. **5**, 279 (2014).

[27] D. Vanderbilt, Phys. Rev. B **41**, 7892(R) (1990).

[28] A. Filippetti, C. D. Pemmaraju, S. Sanvito, P. Delugas, D. Puggioni, and V. Fiorentini, Phys. Rev. B **84**, 195127 (2011); A. Filippetti and N. A. Spaldin, *ibid.* **67**, 125109 (2003); A. Filippetti and V. Fiorentini, Eur. Phys. J. B **71**, 139 (2009).

[29] Y. Kawamura, H. Mashiyama, and K. Hasebe, J. Phys. Soc. Jpn. **71**, 1694 (2002).

[30] C. C. Stoumpos, C. D. Malliakas, and M. G. Kanatzidis, Inorg. Chem. **52**, 9019 (2013).

[31] T. Baikie, Y. Fang, J. M. Kadro, M. Schreyer, F. Wei, S. G. Mhaisalkar, M. Grätzel, and T. J. White, J. Mater. Chem. A **1**, 5628 (2013).

[32] V. M. Goldschmidt, Naturwissenschaften **14**, 477 (1926).

[33] *Handbook of Optical Constants of Solids*, edited by E. D. Palik (Academic Press, New York, 1985).

[34] $A = \alpha L/2.303$, where L is the film thickness, and the factor 2.303 converts from natural to common logarithm.

[35] C. Piliego, M. Manca, R. Kroon, M. Yarema, K. Szendrei, M. R. Andersson, W. Heissc, and M. A. Loi, J. Mater. Chem. **22**, 24411 (2012).

[36] D. V. Talapin and C. B. Murray, Science **310**, 86 (2005).

[37] R. Debnath, O. Bakrbc, and E. H. Sargent, Energy Environ. Sci. **4**, 4870 (2011).

[38] K. S. Jeong, J. Tang, H. Liu, J. Kim, A. W. Schaefer, K. Kemp, L. Levina, X. Wang, S. Hoogland, R. Debnath, L. Brzozowski, E. H. Sargent, and J. B. Asbur, ACS Nano **6**, 89 (2012).